Background γ-rays from Calibration Source Stored Above the Detector SNO-STR-92-065

I. Stairs, P. Skensved and B. C. Robertson

September 16, 1992

Calibration sources for the Sudbury Neutrino Observatory, such as the ^{252}Cf spontaneous fission source, may produce γ-rays with a wide range of energies. There is a possibility that the ^{252}Cf source will be stored in the deck area above the detector, either directly overhead or off to one side. In either case, it is necessary to know the number of high-energy γ-rays reaching the D_2O from the source, since such photons may disintegrate deuterons (neutral-current background) or produce Compton-scattered electrons (charged-current and elastic-scattering backgrounds).

A spectrum (1) of the γ-rays produced by ^{252}Cf is shown in Figure 1, and a table of the γ-ray production rates used in later calculations is given in Appendix A.

Analytical calculations of the attenuations of γ-rays produced by a source at the top of the neck of the detector were performed by David Buchan (2) using the detector geometry shown in Figure 2. Only γ-rays of integral initial energies from 1 to 8 MeV were considered. These calculations were repeated with the air in the neck of the detector replaced by a vacuum to verify that this would be an acceptable approximation in a Monte Carlo simulation. The results of both sets of computations appear in Appendix B.

Such analytical calculations yield only the number of γ-rays of the original energy which survive the passage through the detector. Their results do not include lower-energy photons which arise from the interactions of the high-energy γ-rays with the detector materials.

To obtain more complete results, a Monte Carlo simulation was performed using the EGS4 (Electron-Gamma Ray-Shower, version 4) code (3). The geometry chosen to represent the detector is depicted in Figure 3. Gamma-ray showers with integral initial energies were started at the top of the neck of the detector.

The original intention was to histogram all γ-rays with energies greater than or equal to 2 MeV crossing the boundary of the D_2O. However, because of the large distances involved, very few γ-rays survived the passage through the detector. In order to cut down on the required computer time, several spherical histogramming shells, concentric with the acrylic vessel, were placed between the vacuum-filled neck and the D_2O, and the

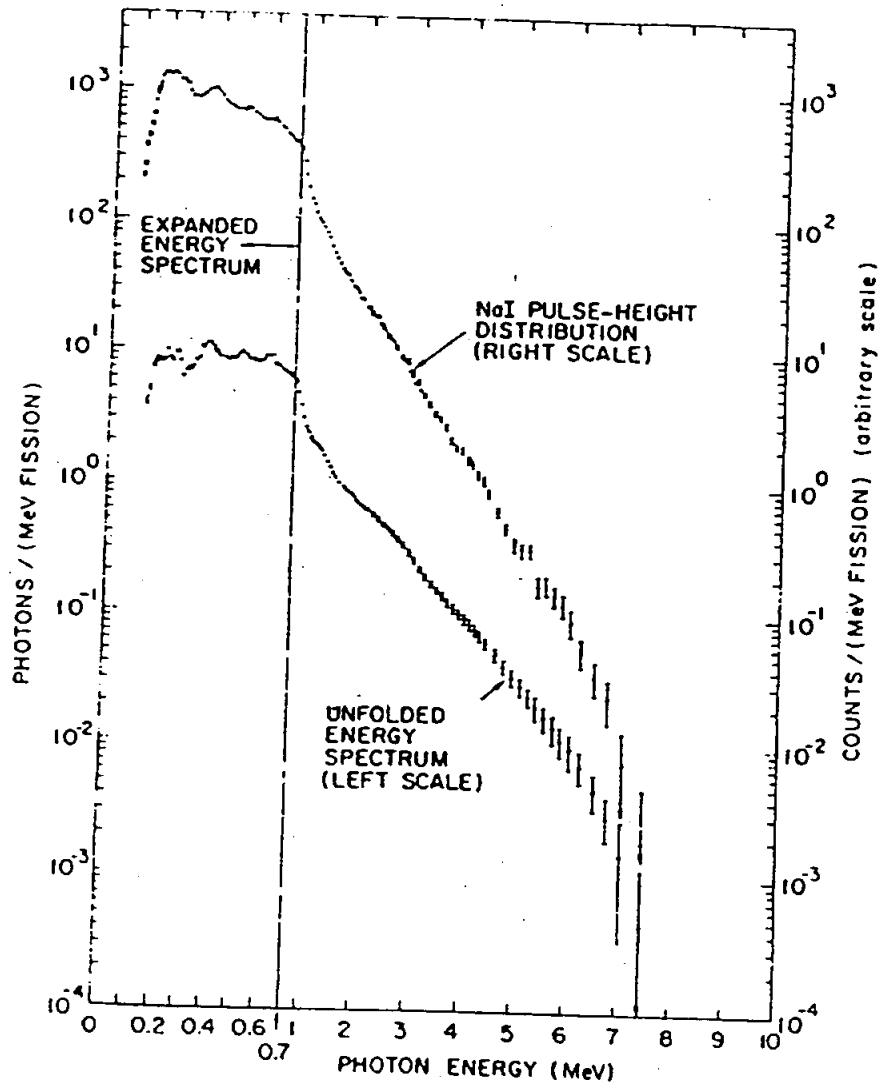

Figure 1: γ-ray spectrum of ^{252}Cf

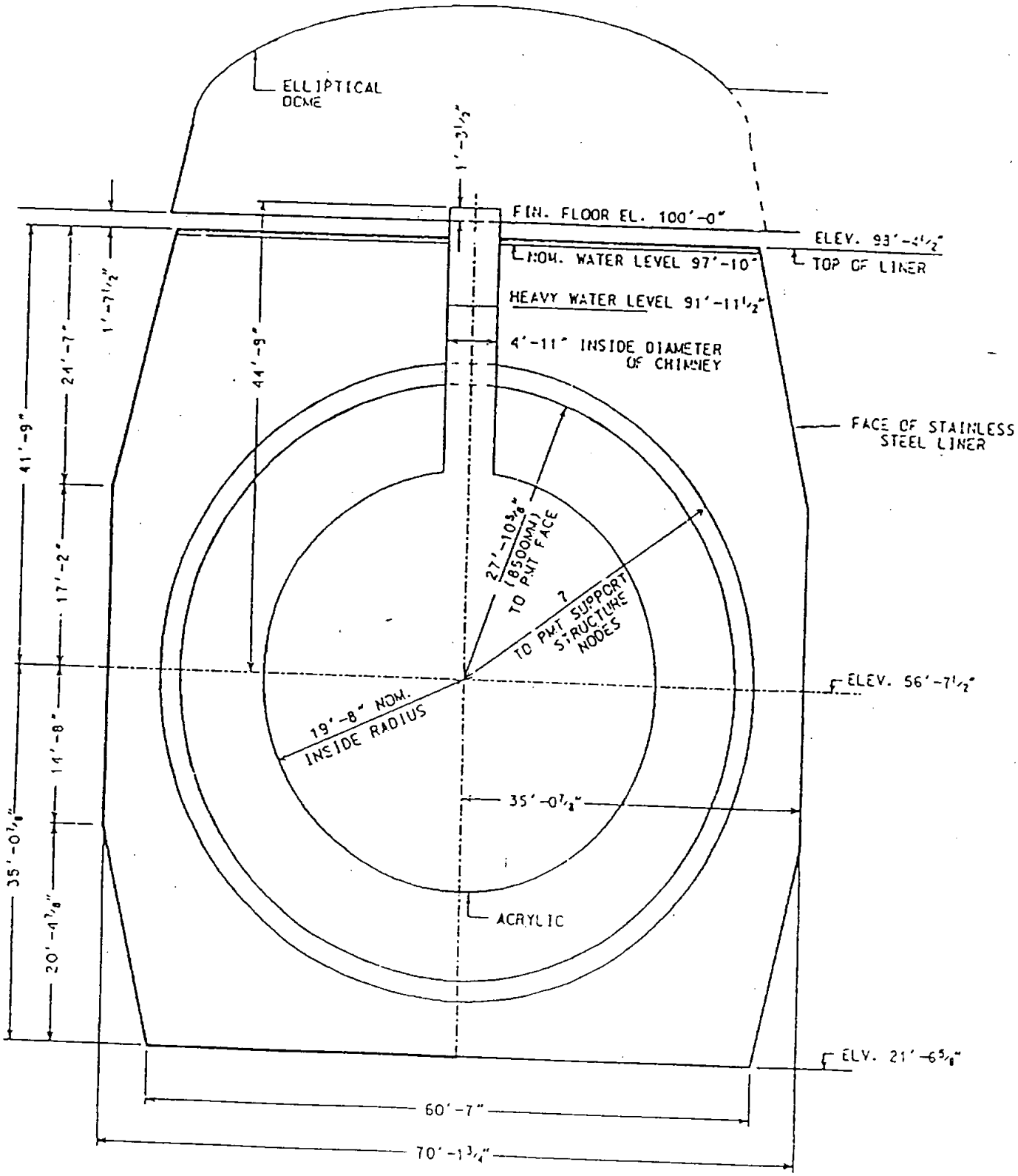

DETECTOR DIMENSIONS

6/03/91

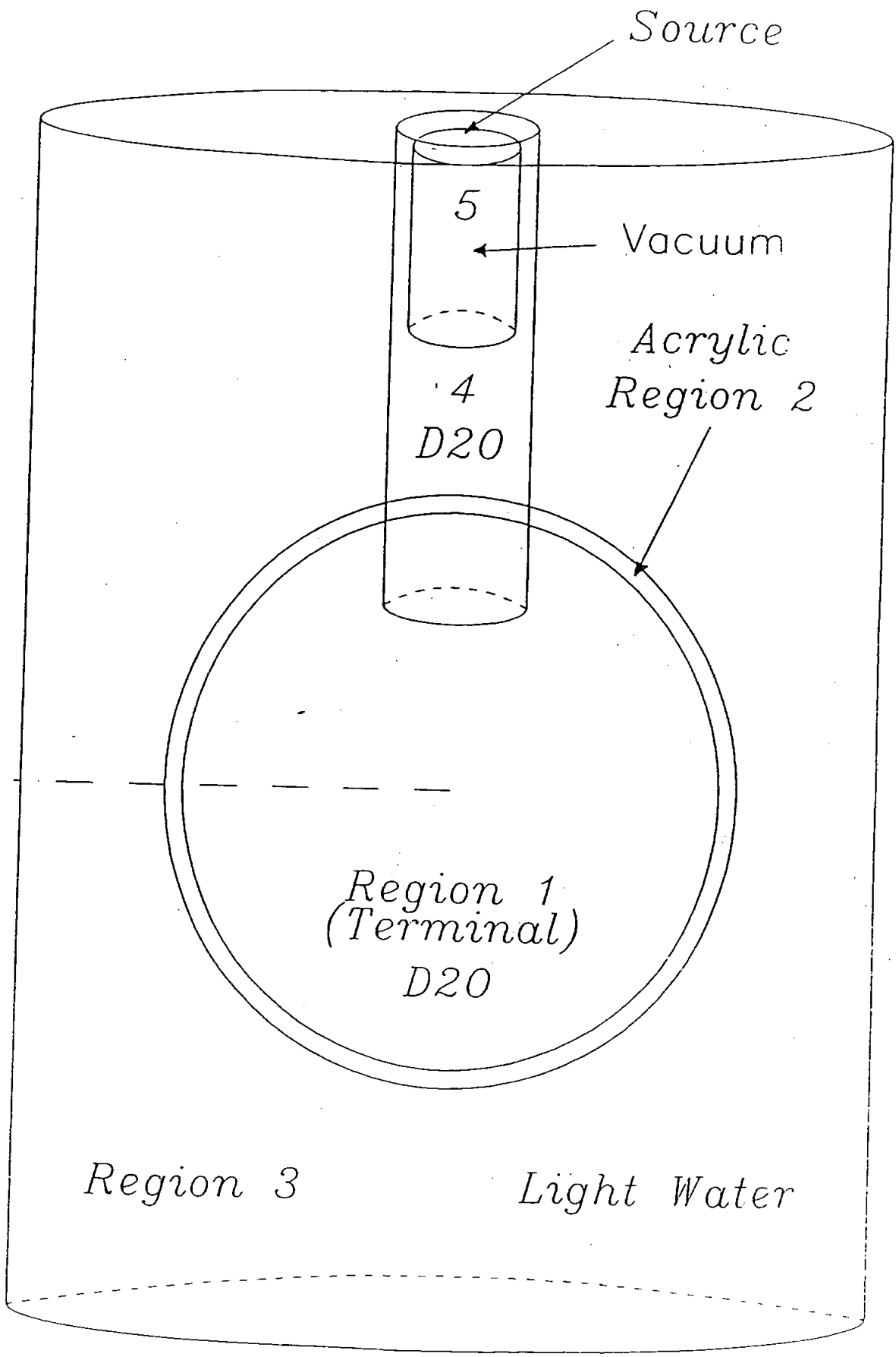
Source
5
Vacuum
Acrylic
Region 2
4
D20
Region 1
(Terminal)
D20
Region 3
Light Water

	D_2O	Acrylic
^{232}Th conc. (g/g)	11×10^{-15}	1.9×10^{-12}
^{238}U conc. (g/g)	11×10^{-15}	3.6×10^{-12}
^{212}Bi β-γs/year	904596	4687454
^{228}Ac β-γs/year	1413444	7324212
^{234}Pa β-γs/year	4315465	42370022

As some of the elements undergo many decays per year, and computer time considerations made running more than 5,000,000 showers per simulation impractical, fewer than a year's worth of showers were started in some cases. The fractions of one year's decays that were run are shown in Table 2.

Table 2: Fractions of one year's decays simulated

Element	D_2O	Acrylic
^{212}Bi	1.0000	1.0000
^{228}Ac	3.5375	0.5000
^{234}Pa	1.0000	0.1000

The resulting plots are shown in Figures 1 through 4. Figure 1 is a plot which includes only ^{208}Tl and ^{214}Bi in the D_2O and acrylic curves. Figure 2 shows the sums of all five elements in the curves. Figure 3 shows the complete acrylic curve and separate plots of ^{212}Bi, ^{228}Ac and ^{234}Pa in the D_2O. In Figure 4, the D_2O curve includes all elements, while the three new elements are plotted separately for the acrylic.

In both the D_2O and the acrylic, the ^{234}Pa makes a significant contribution to the total background at 1.5 MeV, increasing the acrylic ^{208}Tl + ^{214}Bi total by about 40% and increasing the corresponding D_2O figure by about 30%. The other two isotopes are not as important. At 2.5 MeV and higher energies, none of the three new isotopes adds much to the totals. Because of the large ^{234}Pa contribution at 1.5 MeV, the acrylic background now dominates that from the D_2O at all energies.

γrays with energies greater than or equal to 2 MeV crossing these shells were counted. (Electrons and positrons were tracked until their energies dropped below 2 MeV, but were not histogrammed.) The number of γ-rays crossing a shell was assigned its own square root as a standard deviation. Weighted linear regression was then performed on the logarithms of the numbers crossing the shells to determine how many γ-rays would enter the D_2O. These numbers were then divided by the total number of showers initiated (5,000,000 isotropically-distributed showers at each energy) to calculate the attenuation factors. The numbers of γ-rays reaching the D_2O per year were computed by multiplying the attenuation factors by the source strength (57500 fissions/second, derived from the manufacturer's specifications (4)) and by the numbers of γ-rays produced per Mev-fission (see Appendix A).

Due to a lack of time, David Buchan did not complete the simulation. The program has now been finalized, and results for a source at the top of the neck of the detector are given in Table 1.

Table 1: Number of γ-rays reaching the D_2O per year for a ^{252}Cf source at the top of the neck of the detector

Source Energy (MeV)	Attenuation Factors		γ-rays/year	
	At Original Energy	All Energies $\geq$ 2 MeV	At Original Energy	All Energies $\geq$ 2 MeV
3	$(6.2\pm2.9) \times 10^{-11}$	$(1.17\pm0.16) \times 10^{-9}$	23±11	425±58
4	$(1.20\pm0.17) \times 10^{-9}$	$(2.64\pm0.24) \times 10^{-8}$	196±28	4310±390
5	$(7.11\pm0.77) \times 10^{-9}$	$(1.40\pm0.10) \times 10^{-7}$	258±28	5080±360
6	$(2.74\pm0.25) \times 10^{-8}$	$(4.58\pm0.26) \times 10^{-7}$	447±41	7480±420
7	$(7.17\pm0.55) \times 10^{-8}$	$(1.03\pm0.05) \times 10^{-6}$	182±14	2620±130
8	$(1.51\pm0.10) \times 10^{-7}$	$(1.86\pm0.09) \times 10^{-6}$	55±4	675±33

A rough differential spectrum was created by distributing equally, among all energies between 2 MeV and the source energy, the number of γ-rays reaching the D_2O at energies lower than that of the source. The resulting spectrum is shown in Table 2.

Table 2: Differential spectrum of γ-rays reaching the D_2O for a ^{252}Cf source at the top of the neck of the detector

Energy (MeV)	γ-rays/year
2	6420±270
3	6040±230
4	4150±170
5	2610±120
6	1040±50
7	286±15
8	55±4

The attenuation factors and numbers of γ-rays per year for the original energies agree very well with the analytical results given in Appendix B. The program may therefore be used with confidence for sources at different positions.

The simulation was repeated with the source at the edge of the neck of the detector (coordinates (75, 0, 1255.98) cm, taking the centre of the acrylic vessel as the origin) and one metre from the neck (coordinates (175, 0, 1255.98) cm). Since the largest numbers of counts per year were obtained from the showers of 4, 5, 6 and 7 MeV initial energies, only these energies were used in the later simulations. It was also necessary to add more histogramming shells to obtain better statistics. The results of these calculations are given in the next few tables.

Table 3: Number of γ-rays reaching the D_2O per year for a ^{252}Cf source at (75, 0, 1255.98) cm

Source Energy (MeV)	Attenuation Factors		γ-rays/year	
	At Original Energy	All Energies $\geq$ 2 MeV	At Original Energy	All Energies $\geq$ 2 MeV
4	$(3.79\pm0.39) \times 10^{-10}$	$(1.15\pm0.08) \times 10^{-8}$	62±6	1880±140
5	$(2.15\pm0.19) \times 10^{-9}$	$(5.73\pm0.35) \times 10^{-8}$	78±7	2080±130
6	$(1.00\pm0.07) \times 10^{-8}$	$(2.03\pm0.10) \times 10^{-7}$	164±12	3320±160
7	$(2.50\pm0.17) \times 10^{-8}$	$(4.57\pm0.21) \times 10^{-7}$	64±4	1161±53

Table 4: Differential spectrum of γ-rays reaching the D_2O for a ^{252}Cf source at (75, 0, 1255.98) cm

Source Energy (MeV)	γ-rays/year
2	2585 ± 92
3	2585 ± 92
4	1738 ± 60
5	1087 ± 42
6	384 ± 16
7	64 ± 4

Table 5: Number of γ-rays reaching the D_2O per year for a ^{252}Cf source at (175, 0, 1255.98) cm

Source Energy (MeV)	Attenuation Factors		γ-rays/year	
	At Original Energy	All Energies $\geq$ 2 MeV	At Original Energy	All Energies $\geq$ 2 MeV
4	$(2.9\pm4.8) \times 10^{-13}$	$(6.7\pm5.5) \times 10^{-12}$	0.05±0.08	1.09±0.90
5	$(5.2\pm5.2) \times 10^{-12}$	$(5.3\pm2.8) \times 10^{-11}$	0.19±0.19	1.9±1.0
6	$(3.4\pm2.5) \times 10^{-11}$	$(3.1\pm1.2) \times 10^{-10}$	0.56±0.41	5.1±2.0
7	$(1.03\pm0.55) \times 10^{-10}$	$(2.27\pm0.60) \times 10^{-9}$	0.26±0.14	5.8±1.5

Table 6: Differential spectrum of γ-rays reaching the D_2O for a ^{252}Cf source at (175, 0, 1255.98) cm

Source Energy (MeV)	γ-rays/year
2	3.3 ± 0.8
3	3.3 ± 0.8
4	2.9 ± 0.7
5	2.5 ± 0.6
6	1.4 ± 0.5
7	0.3 ± 0.1

It is clear that the number of γ-rays reaching the heavy water per year decreases rapidly for a source away from the neck of the detector. In fact, at a distance of one metre from the edge of the neck, the ^{252}Cf source will no longer pose a problem.

One may also wish to consider other γ-ray sources positioned above the detector. The γ-ray spectra will, of course, vary for different elements, but the attenuation factors tabulated in this report may still be used. To increase the amount of information that may be obtained about the spectra of γ-rays reaching the D_2O, additional attenuation factors have been calculated for all previously-considered starting energies and source positions. These attenuation factors include all γ-rays with energies above 2.2 MeV and, where applicable, above 5 MeV. Combined with the factors listed above, these will yield a more detailed differential spectrum. All these attenuation factors are presented in Appendix C.

Conclusion:

The analytical calculation and the Monte Carlo simulation are in good agreement for a source placed at the top of the neck of the detector, and this similarity justifies the use of the program for sources located in other positions at the top of the detector. The results of such computations indicate that if the ^{252}Cf calibration source is stored one metre from the edge of the neck, the number of fission γ-rays reaching the heavy water per year will be negligibly small.

Although the initial aim of this project was to determine the number of ^{252}Cf fission γ-rays reaching the D_2O for different source positions, the attenuation factors calculated in the process can be applied to γ-rays from any source situated at the top of the detector. With the multiple attenuation factors computed for each source position and starting energy, it should be possible to obtain fairly detailed differential γ-ray spectra.

It would be desirable to reduce the (sometimes very large) uncertainties in the attenuation factors. This could be accomplished by further increasing the number of histogramming shells, by initiating more showers at each energy or by using weight-splitting techniques.

Appendix A: γ-rays per MeV·fission for ^{252}Cf

These values are read from the spectrum in Figure 1.

Energy	γs/MeV·fission
1	2.1
2	0.7
3	0.2
4	0.09
5	0.02
6	0.009
7	0.0014
8	0.0002

Appendix B: Results of the Analytical Calculations

Table B1: Attenuation factors for γ-rays of different starting energies

Energy (MeV)	Attenuation Coefficients (cm^2/g)		Attenuation Factors
	Air	Water	
1	0.064	0.070	1.65×10^{-17}
2	0.045	0.049	5.19×10^{-13}
3	0.036	0.039	7.53×10^{-11}
4	0.031	0.033	1.53×10^{-9}
5	0.028	0.030	6.93×10^{-9}
6	0.025	0.028	1.90×10^{-8}
7	0.023	0.026	5.26×10^{-8}
8	0.022	0.024	1.46×10^{-7}

Table B2: Number of γ-rays reaching the D_2O per year for a ^{252}Cf source at the top of the neck of the detector

Energy (MeV)	Attenuation Factors	γ-rays/ MeV·fission	γ-rays/year
1	1.65×10^{-17}	2.1	6×10^{-5}
2	5.19×10^{-13}	0.7	0.7
3	7.53×10^{-11}	0.2	27
4	1.53×10^{-9}	0.09	250
5	6.93×10^{-9}	0.02	252
6	1.90×10^{-8}	0.009	310
7	5.26×10^{-8}	0.0014	134
8	1.46×10^{-7}	0.0002	53

Table B3: Number of γ-rays reaching the D_2O per year for a vacuum gap in the neck and a ^{252}Cf source at the top of the neck

Source Energy(MeV)	Attenuation Factors	γ-rays/year
1	1.67×10^{-17}	6×10^{-5}
2	5.24×10^{-13}	0.7
3	7.59×10^{-11}	28
4	1.54×10^{-9}	252
5	6.97×10^{-9}	253
6	1.92×10^{-8}	314
7	5.29×10^{-8}	134
8	1.46×10^{-7}	53

Appendix C: Attenuation Factors

Attenuation factors for a source at (0, 0, 1255.98) cm

Source Energy (MeV)	At Original Energy	All Energies $\geq$ 2 MeV
3	$(6.2 \pm 2.9) \times 10^{-11}$	$(1.17 \pm 0.16) \times 10^{-9}$
4	$(1.20 \pm 0.17) \times 10^{-9}$	$(2.64 \pm 0.24) \times 10^{-8}$
5	$(7.11 \pm 0.77) \times 10^{-9}$	$(1.40 \pm 0.10) \times 10^{-7}$
6	$(2.74 \pm 0.25) \times 10^{-8}$	$(4.58 \pm 0.26) \times 10^{-7}$
7	$(7.17 \pm 0.55) \times 10^{-8}$	$(1.03 \pm 0.05) \times 10^{-6}$
8	$(1.51 \pm 0.10) \times 10^{-7}$	$(1.86 \pm 0.09) \times 10^{-6}$

Source Energy (MeV)	All Energies $\geq$ 2.2 MeV	All Energies $\geq$ 5 MeV
3	$(7.7 \pm 1.1) \times 10^{-10}$	
4	$(2.17 \pm 0.20) \times 10^{-8}$	
5	$(1.213 \pm 0.076) \times 10^{-7}$	$(7.11 \pm 0.77) \times 10^{-9}$
6	$(4.12 \pm 0.24) \times 10^{-7}$	$(7.58 \pm 0.58) \times 10^{-8}$
7	$(9.47 \pm 0.48) \times 10^{-7}$	$(2.76 \pm 0.17) \times 10^{-7}$
8	$(1.734 \pm 0.078) \times 10^{-6}$	$(6.48 \pm 0.34) \times 10^{-7}$

Attenuation factors for a source at (75, 0, 1255.98) cm

Source Energy (MeV)	At Original Energy	All Energies $\geq$ 2 MeV
4	$(3.79 \pm 0.39) \times 10^{-10}$	$(1.15 \pm 0.08) \times 10^{-8}$
5	$(2.15 \pm 0.19) \times 10^{-9}$	$(5.73 \pm 0.35) \times 10^{-8}$
6	$(1.00 \pm 0.07) \times 10^{-8}$	$(2.03 \pm 0.10) \times 10^{-7}$
7	$(2.50 \pm 0.17) \times 10^{-8}$	$(4.57 \pm 0.21) \times 10^{-7}$

Source Energy (MeV)	All Energies $\geq$ 2.2 MeV	All Energies $\geq$ 5 MeV
4	$(8.99 \pm 0.65) \times 10^{-9}$	
5	$(4.93 \pm 0.30) \times 10^{-8}$	$(2.15 \pm 0.19) \times 10^{-9}$
6	$(1.829 \pm 0.093) \times 10^{-7}$	$(2.92 \pm 0.19) \times 10^{-8}$
7	$(4.41 \pm 0.20) \times 10^{-7}$	$(1.096 \pm 0.061) \times 10^{-7}$

Attenuation factors for a source at (175, 0, 1255.98) cm

Source Energy (MeV)	At Original Energy	All Energies $\geq$ 2 MeV
4	$(2.9 \pm 4.8) \times 10^{-13}$	$(6.7 \pm 5.5) \times 10^{-12}$
5	$(5.2 \pm 5.2) \times 10^{-12}$	$(5.3 \pm 2.8) \times 10^{-11}$
6	$(3.4 \pm 2.5) \times 10^{-11}$	$(3.1 \pm 1.2) \times 10^{-10}$
7	$(1.03 \pm 0.55) \times 10^{-10}$	$(2.27 \pm 0.60) \times 10^{-9}$

Source Energy (MeV)	All Energies $\geq$ 2.2 MeV	All Energies $\geq$ 5 MeV
4	$(6.2 \pm 5.3) \times 10^{-12}$	
5	$(4.8 \pm 2.6) \times 10^{-11}$	$(5.2 \pm 5.2) \times 10^{-12}$
6	$(2.9 \pm 1.1) \times 10^{-10}$	$(5.6 \pm 3.4) \times 10^{-11}$
7	$(2.13 \pm 0.57) \times 10^{-9}$	$(8.6 \pm 3.2) \times 10^{-10}$

References

(1) V. V. Verbinski, Hans Weber and R. E. Sund, "Prompt Gamma-Rays from $^{235}U(n,f)$, $^{239}Pu(n,f)$ and Spontaneous Fission of ^{252}Cf ", Phys. Rev. C, vol. 7, pp 1173-1185, March 1973.

(2) David Buchan, "Effect on Background of Calibration Source Storage at SNO", Engineering Physics Thesis, Queen's University, March 1992.

(3) W. R. Nelson et al., SLAC-Report-265, Stanford Linear Accelerator Center, December 1985.

(4) Amersham Canada Ltd., Radiation Sources for Industrial Gauging and Analytical Instrumentation, product catalogue, 1985.